Supporting Information for "Quantifying channel steepness distortion resulting from rainfall gradients and concavity changes"

Marina Ruiz Sánchez-Oro[1], Simon M. Mudd[1], and Boris Gailleton[2]

[1]School of GeoSciences, University of Edinburgh, Edinburgh, UK

[2]CNRS, Rennes, France

Contents of this file

1. Text S1 to S6
2. Figures S1 to S19
3. Tables S1 to S9

Introduction This supporting information document contains the derivation of the distortion metrics used in the main text. In addition we present the model parameters and lithologic scenarios. We also provide additional figures for distortion as a function of the change in rainfall as well as for different scenarios of the concavity index.

Text S1. Calculation of k_{sn} distortion

Distortions in the local values of k_{sn} can affect the interpretation of the tectonic and erosional history of a landscape (e.g. Kirby & Whipple, 2012). In order to measure the extent of the k_{sn} distortion caused by different θ values, or alternatively application of

either discharge or area driven calculation of the χ metric, we follow a method similar to that described by (Gailleton et al., 2021).

For the equations below, we compare values in two areas within the same catchment and take the median value of all the $k_s n$ values within that area. The equations below are then quoted in terms of medians instead of absolute values, as was originally devised by (Gailleton et al., 2021).

We start by defining $k_s n$ at two points in the catchment, defined by their median slope and drainage area. We label these points M and N, and use subscripts to denote which point is being analysed:

$$k_M = S_M A_M^\theta \tag{S1}$$

and

$$k_N = S_N A_N^\theta \tag{2}$$

We then take the ratio between the two values of $k_s n$, this we call $r_{k,\theta}$.

$$r_{k,\theta} = \frac{S_M A_M^\theta}{S_N A_N^\theta} \tag{3}$$

To simplify the equation, we can express the drainage area and the slope ratios as r_S and r_A^θ:

$$r_{k,\theta} = r_S r_A^\theta \tag{4}$$

Since we are investigating the effect of varying the concavity between two θ values, we can define:

$$\Delta\theta = \theta_2 - \theta_1 \tag{5}$$

Transforming this into natural log space, we can then see the linear relations between the terms. Note that only the drainage area ratios depend on the concavity θ, which allows us to remove the dependence on the slope ratios, r_S.

$$ln[r_{k,\theta_2}] - ln[r_{k,\theta_1}] = ln[r_S] + \theta_2 ln[r_A] - ln[r_S] - \theta_1 ln[r_A] \tag{6}$$

$$ln[r_{k,\theta_2}] - ln[r_{k,\theta_1}] = \Delta\theta ln[r_A] \tag{7}$$

Finally, we can rewrite this ratio of ratios as a distortion originated from the variation in θ values.

$$\beta(\Delta\theta) = \frac{r_{k,\theta_2}}{r_{k,\theta_1}} = r_A^{\Delta\theta} \tag{8}$$

We then use these equations with the following series of steps in order calculate the degree of distortion in k_{sn} values that may be introduced by selection of the wrong method of calculating χ (for example, using A to calculate χ_A when incision depends on Q).

1. We select tributaries based on the drainage area: normalise the drainage area (DA^*) to be able to establish a common threshold for all the basins.

2. We remove the pixels that have a $DA^* < 0.1$.

3. We choose the pixels corresponding to larger rivers ($DA^* > 0.8$) and those belonging to side tributaries ($DA^* < 0.3$).

4. We normalise the k_{sn} values by the largest value in each basin.

5. We take the median value of the k^*_{sn} values for the smaller and the larger tributaries.

6. We calculate the ratio between the two medians (large DA/small DA).

These calculations are aimed at quantifying the distortion in k_sn related to a change in concavity index, θ. To study the distortion incurred by a change in incision rule (i.e. using discharge instead of drainage area) we need to introduce a further variable. We express discharge as $Q = RA$, where R is the rainfall rate (m/yr). The framework is the same, but we define the discharge k_{sn} ratio as:

$$r_{k,\theta,Q} = \frac{S_M(R_M A_M)^\theta}{S_N(R_N A_N)^\theta} \tag{9}$$

which we express as

$$r_{k,\theta,Q} = r_S(r_R r_A)^\theta \tag{10}$$

To see the distortion caused by the inclusion of rainfall in the calculations we take the ratio between r_k and $r_{k,Q}$:

$$r_{k,\theta,Q} = \frac{r_S(r_R r_A)^\theta}{r_s r_A^\theta} \tag{11}$$

If we assume a constant value for θ, the equation becomes:

$$\frac{r_{k,\theta,Q}}{r_{k,\theta}} = r_R^\theta \tag{12}$$

If we then combine both k_{sn} distortion cases (i.e. change in θ and change in incision rule) together we get the following expressions:

$$\frac{r_{k,Q,\theta_1}}{r_{k,\theta_2}} = \frac{r_S r_R^{\theta_1} r_A^{\theta_1}}{r_S r_A^{\theta_2}} \tag{13}$$

doing the natural log transformation of equation 13 leads to the ratio:

$$\frac{r_{k,Q,\theta_1}}{r_{k,\theta_2}} = r_R^{\theta_1} + r_A^{\Delta\theta} \tag{14}$$

.

Equations 8, 12, and 14 allow us to quantify three varieties of distortion: those caused by changes in θ, those caused by changes in the incision rule, and a combination of both. To capture the variety of distortion we calculate four distortion ratios:

- $\frac{k_{sn}(\theta=\theta_{best})}{k_{sn}(\theta=0.45)}$ (Distortion case i_A)
- $\frac{k_{sn-q}(\theta=\theta_{best})}{k_{sn-q}(\theta=0.45)}$ (Distortion case i_Q)
- $\frac{k_{sn}(\theta=\theta_{best})}{k_{sn-q}(\theta=\theta_{best})}$ (Distortion case ii)
- $\frac{k_{sn}(\theta=0.45)}{k_{sn-q}(\theta=0.45)}$ (Distortion case iii)

A ratio value of 1 means that there is no change in the k_{sn} values being compared, whereas values above or below 1 show a trend in either of the directions.

We always take basin M to be the larger basin. That is, This means that the ratio $A_M/A_N > 1$ in all our calculations. To understand what this means physically, we consider the following scenarios:

- Case a): k_{sn} distortion > 1
- Case b): k_{sn} distortion < 1

In this case, the area M has a larger drainage area than the area N in the calculations. Given this, for Case a), this implies that $\theta_2 > \theta_1$. In Case b), the opposite is true, $\theta_1 > \theta 2$.

When we have only a difference in the incision case, the distortion signal is dominated by the strength of the rainfall gradient. In our set up, the rainfall increases toward the east of the simulation. We will refer to the western-facing basins "dry" and the eastern-facing basins as "wet". In this case, a change of sign in the k_{sn} distortion arises from $R_M/R_N < 1$ on the dry basins and $R_M/R_N > 1$ on the wet basins.

Case *i*: Distortion from changes in θ

Distortion:

$$r_A^{\Delta\theta} = \left(\frac{A_M}{A_N}\right)^{\theta_2-\theta_1} \tag{15}$$

$$\theta_2 > \theta_1 \Rightarrow \left(\frac{A_M}{A_N}\right)^{+} \Rightarrow r_A^{\Delta\theta} > 1 \tag{16}$$

$$\theta_2 < \theta_1 \Rightarrow \left(\frac{A_M}{A_N}\right)^{-} \Rightarrow r_A^{\Delta\theta} < 1 \tag{17}$$

$$\tag{18}$$

Based on the distortion value we can find out what the relationship between the different θ is and vice versa. In our case θ_1 is the numerator and θ_2 the denominator in the 4 distortion ratios above. Larger θ values mean faster change of gradient downstream.

Case *ii*: Distortion from changes in incision rule (rainfall)

In this case, we are not comparing the effect of different θ so we only focus on the rainfall impact. We assume that θ is fixed to some reference value, in this case $\theta = 0.45$.

Distortion:

$$r_R^{\theta} = \left(\frac{R_M}{R_N}\right)^{\theta} \tag{19}$$

As explained above, we reason through this step in terms of dry and wet basins:

$$Dry\ side: R_M < R_N \Rightarrow \left(\frac{R_M}{R_N}\right)^{0.45} < 1 \Rightarrow r_R^\theta < 1 \tag{20}$$

$$Wet\ side: R_M > R_N \Rightarrow \left(\frac{R_M}{R_N}\right)^{0.45} > 1 \Rightarrow r_R^\theta > 1 \tag{21}$$

$$\tag{22}$$

In this case, given the rainfall constraints that we have in the simulations, the maximum value for r_R is 10 (as this is the largest gradient case).

Case *iii*: Distortion from changes in θ and incision rule (due to rainfall)

Distortion:

$$r_R^\theta + r_A^{\Delta\theta} = \left(\frac{R_M}{R_N}\right)^{\theta_1} + \left(\frac{A_M}{A_N}\right)^{\Delta\theta} \tag{23}$$

Always: $A_M > A_N$

Dry: $R_M < R_N$

Wet: $R_M > R_N$

$\theta_1 >> \Delta\theta$

We study the two terms in the distortion equation.

Distortion < 1:

Dry side:

$$\left(\frac{R_M}{R_N}\right)^{0.45} < 1 \tag{24}$$

$$\left(\frac{A_M}{A_N}\right)^{0.45} > 1 \tag{25}$$

$$\tag{26}$$

For the overall distortion to be negative, $\Delta\theta < 0$. So that $\theta_1 > \theta_2$.

Wet side:

$$\left(\frac{R_M}{R_N}\right)^{0.45} > 1 \tag{27}$$
$$\left(\frac{A_M}{A_N}\right)^{0.45} > 1 \tag{28}$$
$$\tag{29}$$

From these parameters, the distortion will never be below 1 in this case for the wet area.

Distortion > 1:

Dry side:

$$\left(\frac{R_M}{R_N}\right)^{0.45} < 1 \tag{30}$$
$$\left(\frac{A_M}{A_N}\right)^{0.45} > 1 \tag{31}$$
$$\tag{32}$$

For the overall distortion to be above 1 for the dry side, $\theta_2 > \theta_1$.

Wet side:

$$\left(\frac{R_M}{R_N}\right)^{0.45} > 1 \tag{33}$$
$$\left(\frac{A_M}{A_N}\right)^{0.45} > 1 \tag{34}$$
$$\tag{35}$$

From these parameters, the distortion in the wet side will always be above 1 in this case for the wet area regardless of θ.

Text S2. Model parameters

For our numerical simulations, we run models using the parameters described in Table S1.

Text S3. Lithologic scenarios

We run simulations with a number of different lithologic scenarios, examples of which are shown in Figure S1.

Dense blob lithology

The drainage area-driven incision is represented in Figure S2A. Compared to Figure S11A, we notice that the distinctions between calculating disorder with and without rainfall are largely masked by the presence of a heterogeneous lithology. In this drainage area-driven case, we would expect that calculating χ_A would lead to higher disorder values than using χ_Q. However, this is not clearly seen, with the results yielding the lowest disorder being mixed.

Even though from the overall behavior it is difficult to pick out the scenario with the least disorder. Looking at individual pairs of basins, we can see a signal. Note that in this case, the basins are identical regardless of the rainfall gradient, as there is only one model evolution. We can see that for each of the basins, the value for the case χ_Q presents higher disorder values than χ_A. In this case, the behaviour of the basins becomes case specific. In S11, A, all basins showed a base disorder close to 0 as there were no forcings present and therefore and consequent disorder calculations with χ_Q shows always higher disorder value regardless of the basin or the rainfall gradient. In this case, however, we

see that the baseline disorder for χ_A has increased from 0 by up to 14% in some basins. We still see, however, that the basins record a lower disorder when χ_A is calculated, as we expect from a drainage area-driven scenario.

In Figure S2B, we can see the effects of adding rainfall. Similarly to Figure S2A, it is very difficult to distinguish the signal from each of the χ cases in terms of the overall behaviour of all the basins in the same simulation run (for each rainfall gradient). If we look at individual basins, however, we see that the disorder is smaller when we use χ_Q for some of the basins.

Blob lithology

We present results from the blob lithology simulations in Figures S5, S6, and S7. The distortions associated with this scenario are shown in Table S7.

Striped Lithology

We present results from the striped lithology simulations in Figures S8, S9, and S10. The distortions associated with this scenario are shown in Table S10.

Text S4. Incision: Drainage Area vs Incision: Discharge

Figure S11 shows how D^* responds to changes in both rainfall gradients and incision rule (one basin is represented by one plot point). In the A-driven incision experiment (top plot), we expect the $\chi_A - z$ profiles to be linear and the associated $\theta_{best,A}$ to be 0.45. The disorder in this case is close to 0 for all the basins in all rainfall instances. In contrast, calculation using χ_Q results in more disorder and values of $\theta_{best,Q}$ that diverge from 0.45, with the differences increasing as the rainfall gradient increases.

Figure S11B portrays the effect of including rainfall in the χ_A calculations, given a Q-driven incision model. In this case, there are as many models as there are rainfall

scenarios, with the first one corresponding to the A-driven incision model with a base rainfall of 1 m/yr and no gradient. Calculating χ_Q with matching incision rule rainfall gradient yields D^* values of 0 compared to calculating χ_A. For instance, in the model run with a rainfall gradient of 5 m/yr, the χ_Q calculations with 5 m/yr will yield a lower disorder than calculating χ_A (without rainfall). This also means that the value for $\theta_{best,Q}$ will be 0.45 in that case. We see that as the rainfall gradient increases the differences between the minimum disorder values increases, and the model behaviour diverges from the A-driven incision case.

Note that in the discharge-driven incision case, the simulated basins vary under each of the rainfall scenarios, showing the differences that different rainfall gradients make in the evolution of basins. In the drainage area incision case we only have one set of simulated basins as the modelling conditions are the same and it is only in the χ calculations that we incorporate a dependence on rainfall.

In the drainage area scenario, the variations in χ_Q and $\theta_{best,Q}$ arise from including a rainfall gradient in the calculations, they are purely a mathematical bias. In the discharge scenarios, changes in χ_Q are captured from changes in the topography of the simulated basins due to the imposed rainfall gradients.

The scale of the change in disorder varies between the two incision scenarios. In the A-driven case (plot A), disorder ranges between less than 0.01 (when calculating χ_A with the 1 m/yr rainfall gradient) and over 0.04 (with a 10 m/yr χ_A calculation). On the other hand, the Q-driven scenario leads to larger disorder changes of one order of magnitude, ranging from 0.01 to 0.14. Thus, when applying disorder minimisation, choosing the

incorrect incision rule leads to stronger variations in optimal θ_best when discharge is the main incision mechanism.

Text S5. Disorder in natural landscapes

Figure S14 shows the values of the minimum D^* points for χ_A and χ_Q for all the selected mountain ranges. We see a resemblance with the model results with heterogeneous lithology, where it is difficult to distinguish whether there is an overall trend suggesting the preference of one incision mechanism over another at a large scale.

The disorder value ranges are considerably larger than those for the model runs. In natural landscapes, the minimum D^* values range between 0.1 and 0.75. We compare this to the minimum D^* from the simulations, where the maximum disorder was 0.4 for the discharge-driven heterogeneous lithology case and 0.14 for the discharge-driven homogeneous lithology case.

We note that basins within the same geographical area have ΔD^* of up to 0.4. The differences when calculating D^* with or without rainfall are one order of magnitude smaller, which makes it challenging to compare the influence of disorder across multiple mountain range of different scales.

Text S6. Effect of varying the concavity index, θ: 0.35 and 0.55

In the following section we explore how choosing $\theta = 0.45$ in a landscape carved by a different m/n ratio affects the k_{sn} distortion. We highlight this case because of the large body of literature that assumes $\theta = 0.45$ when deriving erosion rates and determining the tectonic history of a basin. Figure S16 reflects data run from models with $m/n = 0.35$, where the resulting landscapes show higher relief and straighter rivers than those for $m/n = 0.45$.

The plots from a discharge driven model (Figure S16) suggests that regardless of the incision case chosen, the wrong concavity ($\theta = 0.45$ in this case) will lead to k_{sn} distortions reaching 30% (plots A and B). The ratios are all > 1, which is in line with the mathematical formulation of distortion, given $\theta_1 = 0.35$ and $\theta_2 = 0.45$. Opting for the incorrect incision scenario (Figure S16C) under $\theta = 0.35$ leads to a smaller distortions of up to 13% for the largest rainfall gradient scenario.

This implies that analysing the incision pattern for a landscape where the concavity rule is not constrained, a mistaken choice of $\theta = 0.45$ causes larger distortion than assuming the incorrect incision scenario.

Next we choose $m/n = 0.55$ (Figure S18), which forms a landscape with lower relief and more sinuous rivers than $m/n = 0.45$. The behaviour is similar to that of the $m/n = 0.35$ scenario, but in this case the distortion is < 1 when we compare the effects of choosing 0.45 or 0.55 for θ (Figures S18A and B). There is no change in the distortion values based on the rainfall in Figure S18A and B. The highest distortion occurs when using optimising θ under the incorrect incision scenario (Figure S18D). The maximum distortion originated

from varying the incision rule is lower compared to the other scenarios (Figure S18E, 13% compared to 20-26% in Figures S18A, B, D).

Aside from the distortions in k_{sn} and k_{sn-q}, we also include the distributions of steepness indices under different rainfall, concavity and incision scenarios. In Figure S13, we show the distributions for the cases when the initial $m/n = 0.45$. The absolute channel steepness index values show a bimodal distribution when we use the optimal concavity, but a smoother and narrower monomodal shape when using 0.45. We see that for the A-driven incision, under $\theta = 0.45$, including rainfall gradients in the calculations increases the channel steepness values. When we have the Q-driven incision case, we obtain lower channel steepness values when we do not include rainfall in the calculations. Between the two incision cases, channel steepness is reduced with increased precipitation rates, with variability depending on the values of the concavity, as quantified by (D'Arcy & Whittaker, 2014).

References

D'Arcy, M., & Whittaker, A. C. (2014). Geomorphic constraints on landscape sensitivity to climate in tectonically active areas. *Geomorphology*, *204*, 366–381. doi: 10.1016/j.geomorph.2013.08.019

Gailleton, B., Mudd, S. M., Clubb, F. J., Grieve, S. W., & Hurst, M. D. (2021). Impact of Changing Concavity Indices on Channel Steepness and Divide Migration Metrics. *Journal of Geophysical Research: Earth Surface*, *126*(10). doi: 10.1029/2020JF006060

Kirby, E., & Whipple, K. X. (2012). Expression of active tectonics in erosional landscapes. *Journal of Structural Geology*, *44*, 54–75. doi: 10.1016/J.JSG.2012.07.009

Table S1. Summary of the conditions upon which the distortion in k_{sn} values are above or below 1 for distortion calculated with changes in incision rate and θ.

	DRY	WET
Dist. < 1	$\theta_1 > \theta_2$ AND ratio dependence	ALWAYS
Dist. > 1	ALL θ, ratio dependence	NEVER

Table S2. Model parameters values for the initial conditions of the discharge simulation.

Parameter	Value
Pixel resolution (m)	30
Lx (m)	1.5e4
Ly (m)	3e4
Diamond min height (m)	0
Diamond max height (m)	1
Roughness	0.75
Random seed	420
K $(m^{-1}yr^{-1})$	3e-8
EU (m^{-1})	1e-5
snastm	0.45
n	1

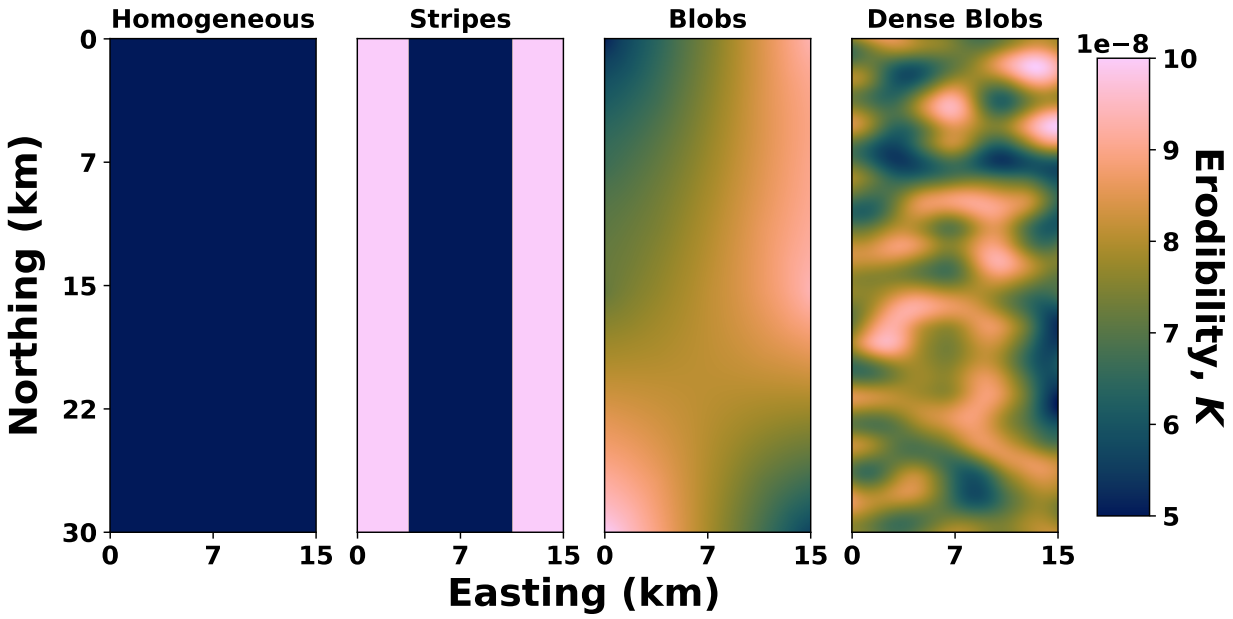

Figure S1. The four types of lithologies modelled: (a) Homogeneous lithology, (b) Striped lithology, (c) blob lithology and (d) dense blob lithology.

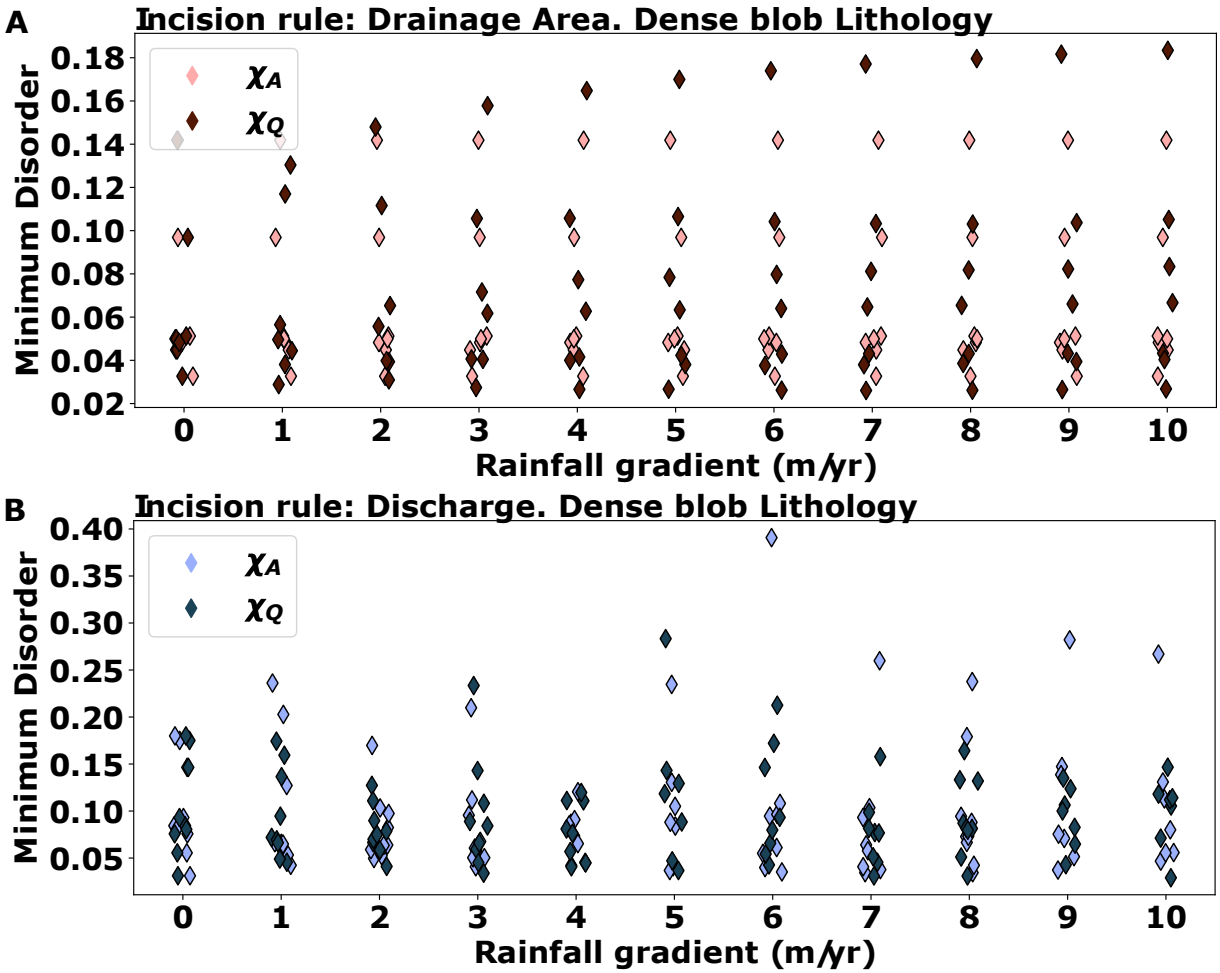

Figure S2. Evolution of the minimum disorder for model runs with drainage area (A) and discharge-driven (B) incision rule for a range of rainfall gradients (0-10m/yr) under dense blob lithology. We show the minimum disorder values when calculating χ_A and χ_Q, for rainfall values increasing from 0 m/yr to 10 m/yr. Under a dense blob lithology it is not possible to establish a pattern in disorder values when using χ_A as opposed to χ_Q, regardless of the incision scenario.

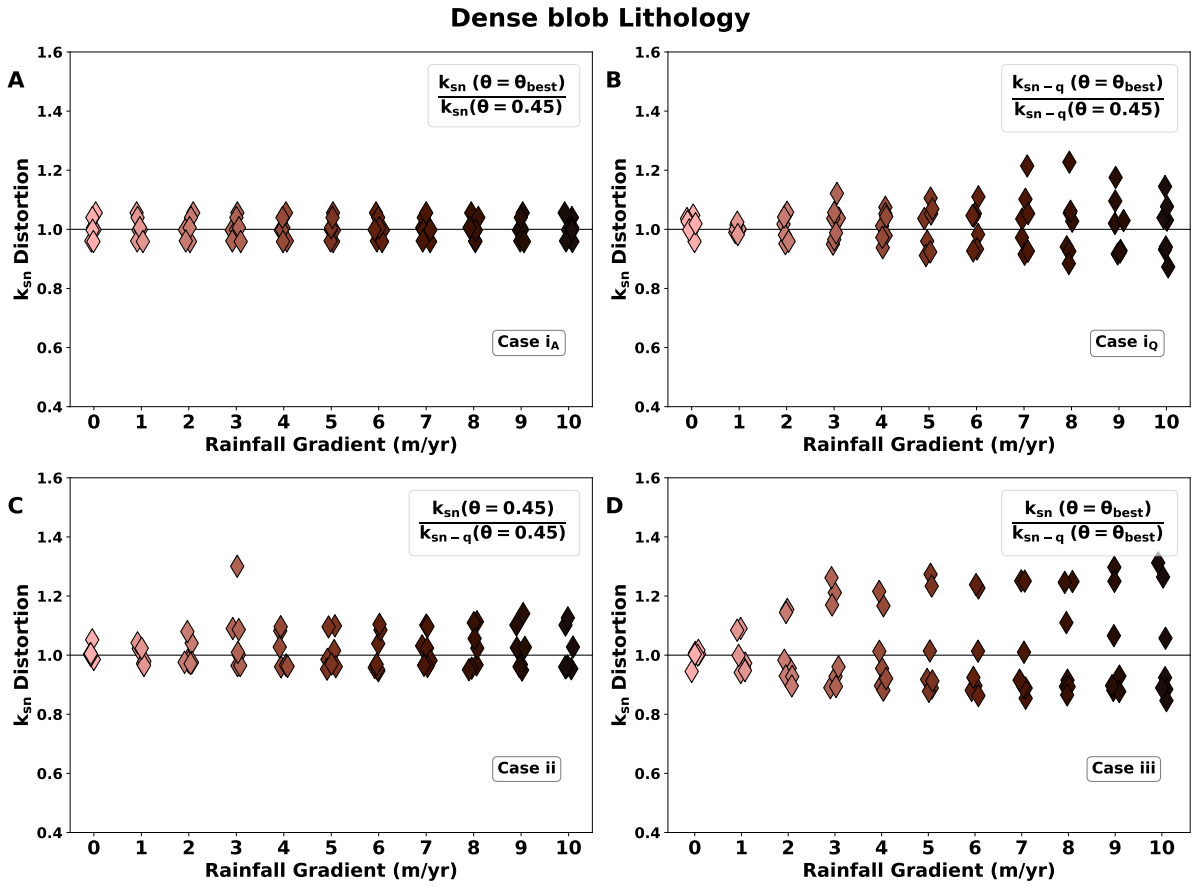

Figure S3. Distortion in k_{sn} for the A-driven incision case under dense blob lithology and initial m/n=0.45. A distortion of 1 (solid black line) keeps the value of k_{sn} unchanged. We show the possible distortion scenarios that one might encounter under different assumptions of concavity index and incision. (A) shows the distortion incurred by not optimising θ under A-driven incision, whereas (B) highlights the effects of optimising concavity under the incorrect incision scenario (discharge), where we see the largest k_{sn} distortions of up to 34%. (C) keeps concavity index at 0.45 but compares incision scenario and (D) comprises the effects of θ optimisation under different assumptions of incision scenarios.

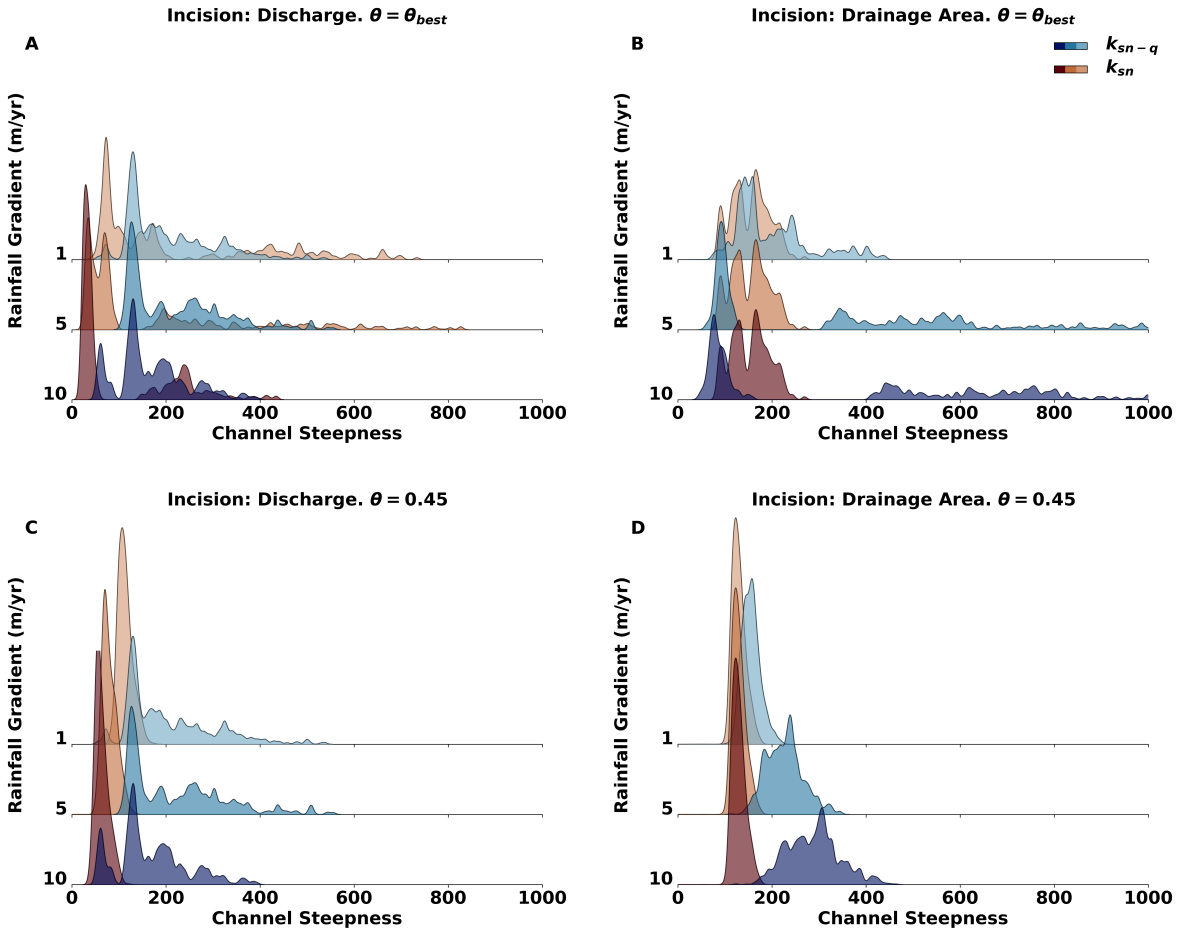

Figure S4. Distribution of k_{sn} and k_{sn-q} values for the basins in the dense blob lithology simulation. (A) and (C) show how the channel steepness distribution remains largely unchanged when using k_{sn-q} but it shifts towards smaller channel when using k_{sn}. (B) and (D) shows a similar trend, but in this case the k_{sn} distributions remain unchanged while the k_{sn-q} as the rainfall is increased.

Table S3. Maximum values of k_{sn} distortion for the dense blob lithology case with $m/n = 0.45$. Bold values indicate the highest distortion for each incision scenario.

Dense Blob Litho.	Case i_A	Case i_Q	Case ii	Case iii
Drainage Area (A)	23%	6%	30%	**31**%
Discharge (Q)	19%	35%	44%	**54**%

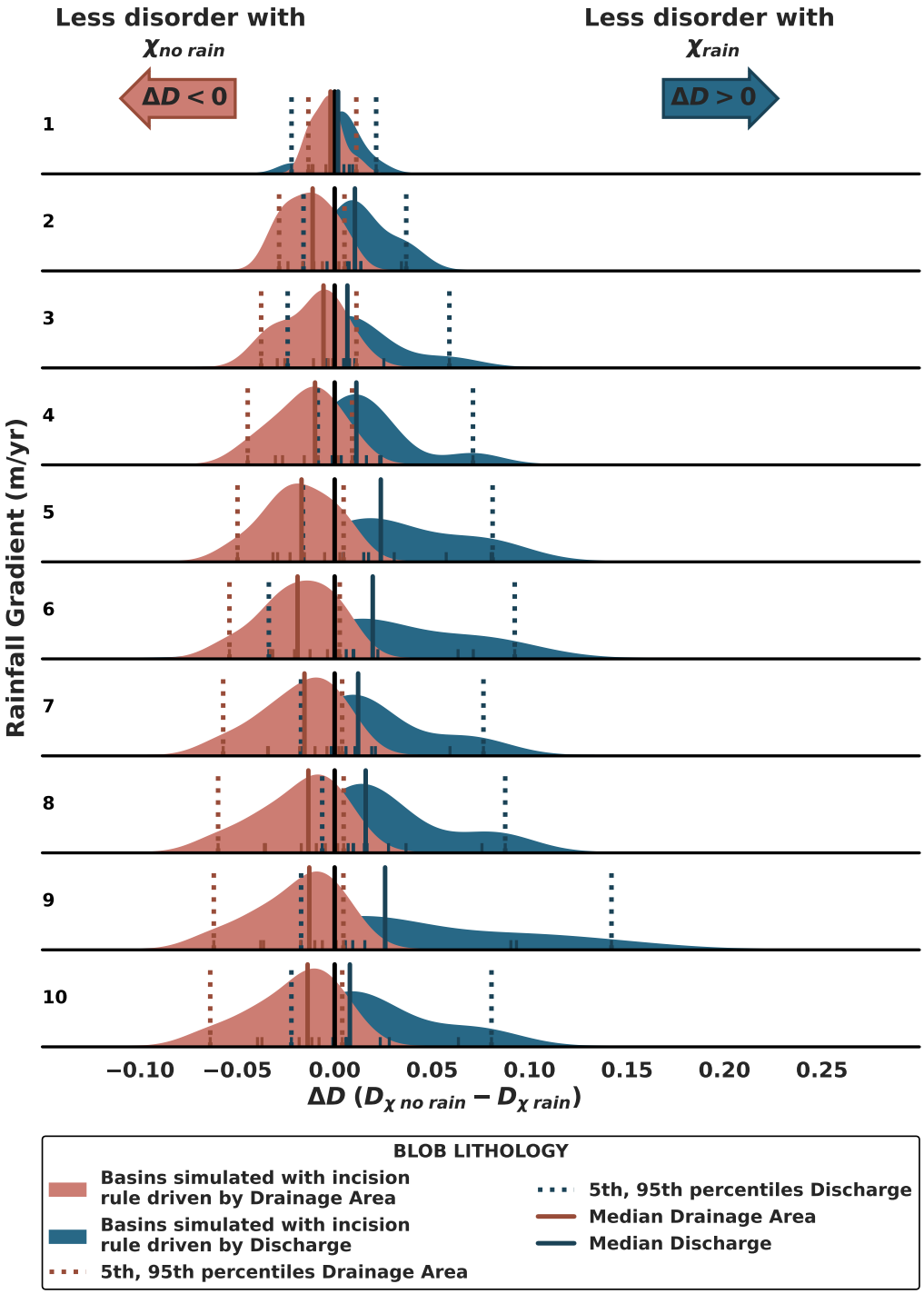

Figure S5. Comparison of the median values for ΔD^* for each of the rainfall ranges for A and Q-driven incision under blob lithology for an initial m/n=0.45. Even though the medians lie at either side of the 0 indicator regardless of the rainfall gradient, it is not possible to establish with 95% that the distributions are distinguishable because the percentiles overlap.

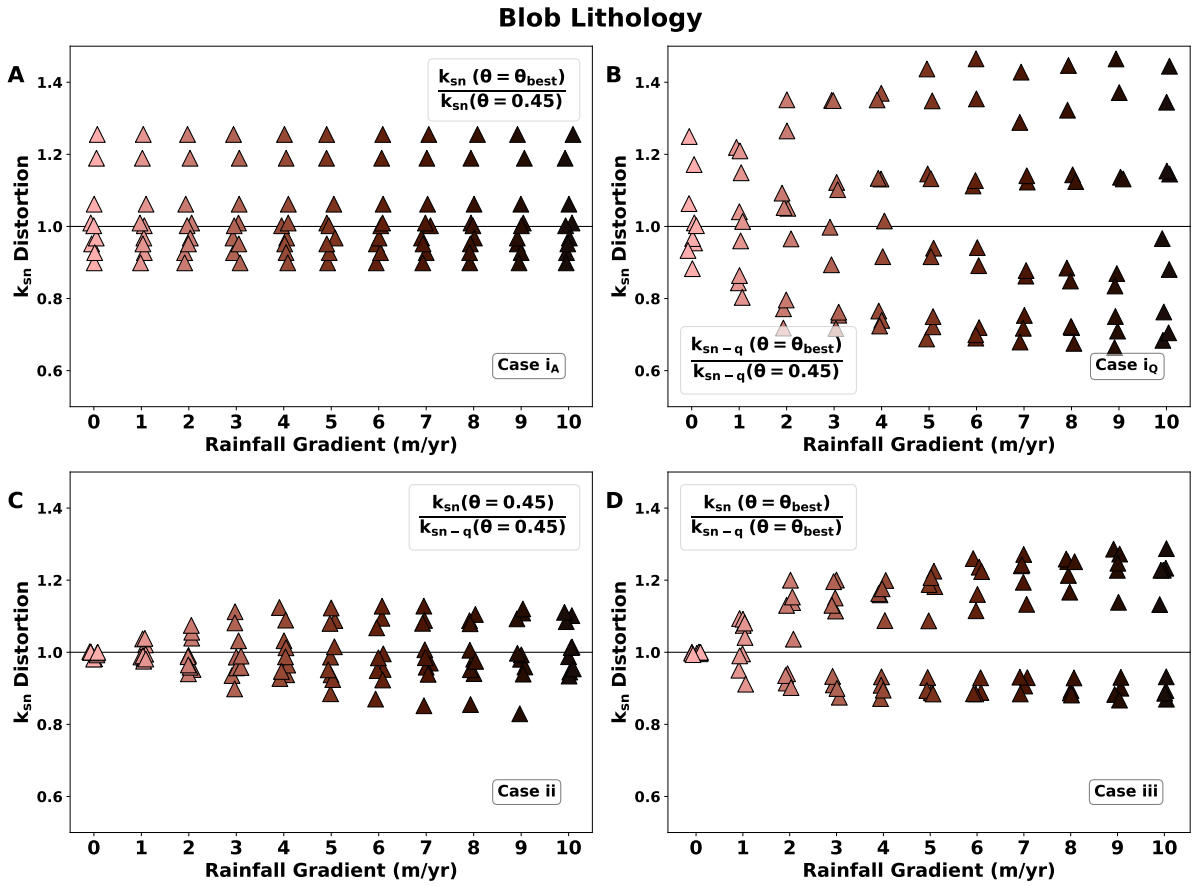

Figure S6. Distortion in k_{sn} for the A-driven incision case under blob lithology and initial m/n=0.45. A distortion of 1 (solid black line) keeps the value of k_{sn} unchanged. We show the possible distortion scenarios that one might encounter under different assumptions of concavity index and incision. (A) shows the distortion incurred by not optimising θ under A-driven incision, where we see the largest k_{sn} distortions of up to 46%. (B) highlights the effects of optimising concavity under the incorrect incision scenario (discharge). (C) keeps concavity index at 0.45 but compares incision scenario and (D) comprises the effects of θ optimisation under different assumptions of incision scenarios.

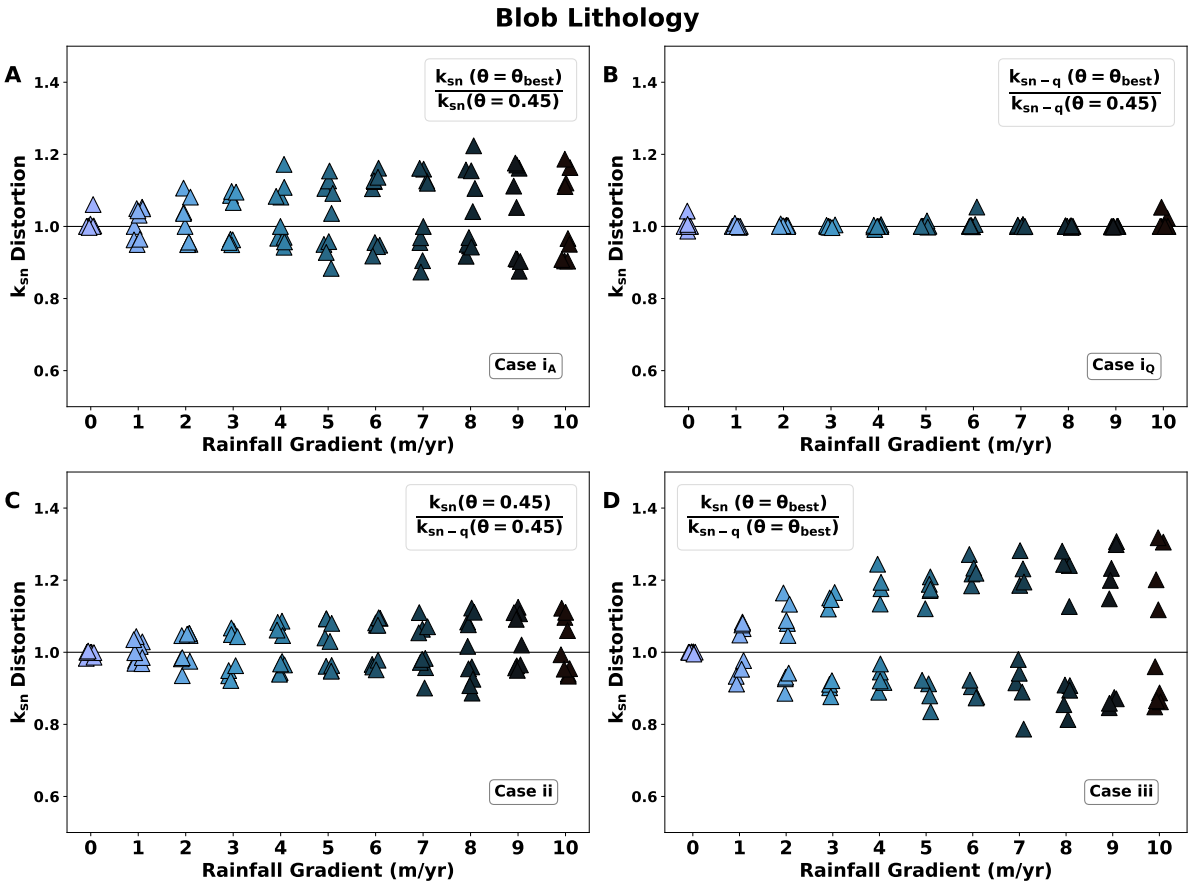

Figure S7. Distortion in k_{sn} for the Q-driven incision case under blob lithology and initial m/n=0.45. A distortion of 1 (solid black line) keeps the value of k_{sn} unchanged. We show the possible distortion scenarios that one might encounter under different assumptions of concavity index and incision. (A) highlights the effects of optimising concavity under the incorrect incision scenario (drainage area), whereas (B) shows the distortion incurred by not optimising θ under Q-driven incision. (C) keeps concavity index at 0.45 but compares incision scenario and (D) comprises the effects of θ optimisation under different assumptions of incision scenarios, where we see the largest k_{sn} distortions of up to 32%.

Table S4. Maximum values of k_{sn} distortion for the blob lithology case with $m/n = 0.45$. Bold values indicate the highest distortion for each incision scenario.

Blob Litho.	Case i_Q	Case i_A	Case ii	Case iii
Drainage Area (A)	**46**%	26%	17%	29%
Discharge (Q)	5%	22%	12%	**32**%

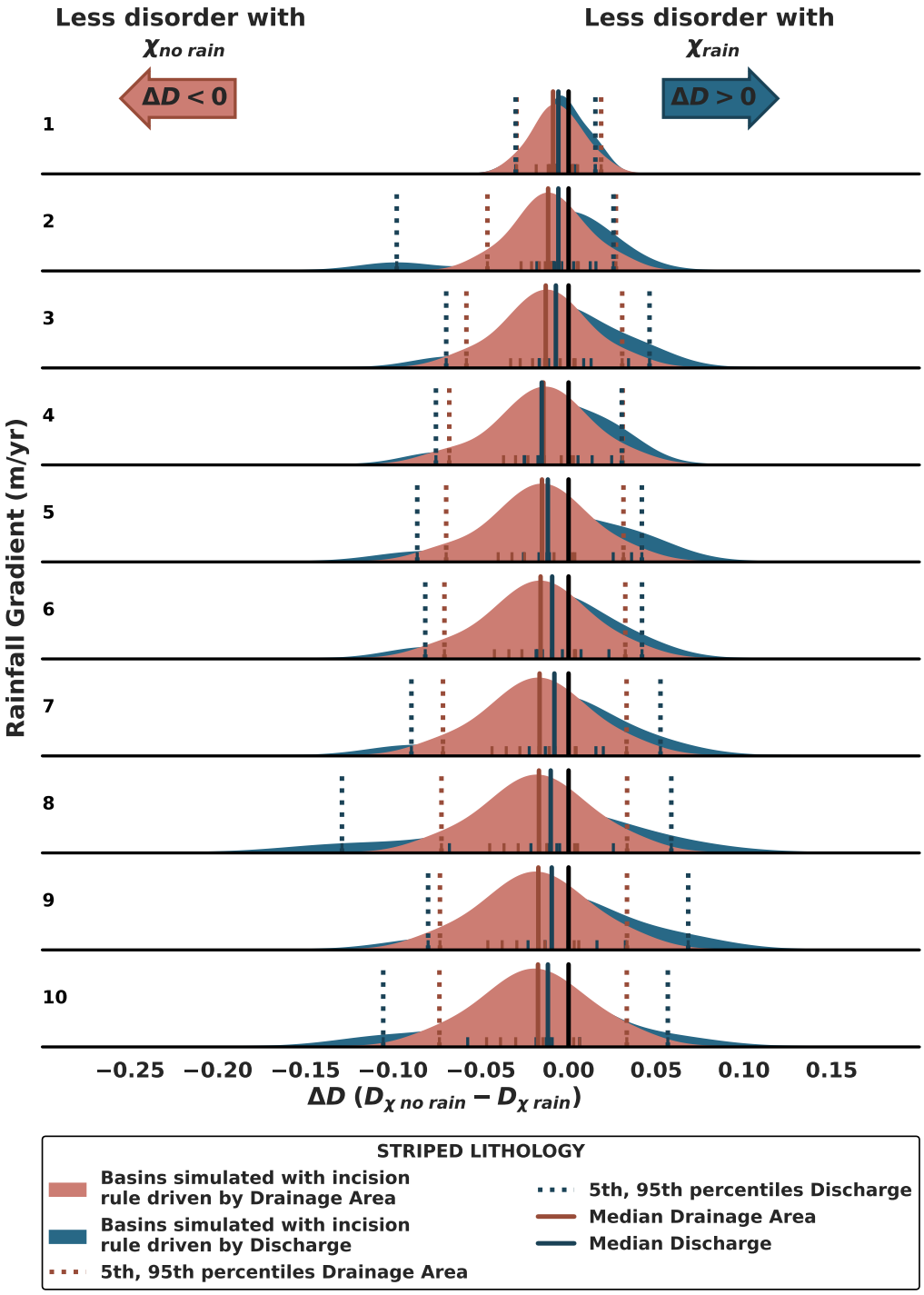

Figure S8. Comparison of the median values for ΔD^* for each of the rainfall ranges for A and Q-driven incision under striped lithology for an initial m/n=0.45. In this case, all medians lie on the negative side of the x-axis, with the percentiles fully overlapping, making the distributions non-distinguishable.

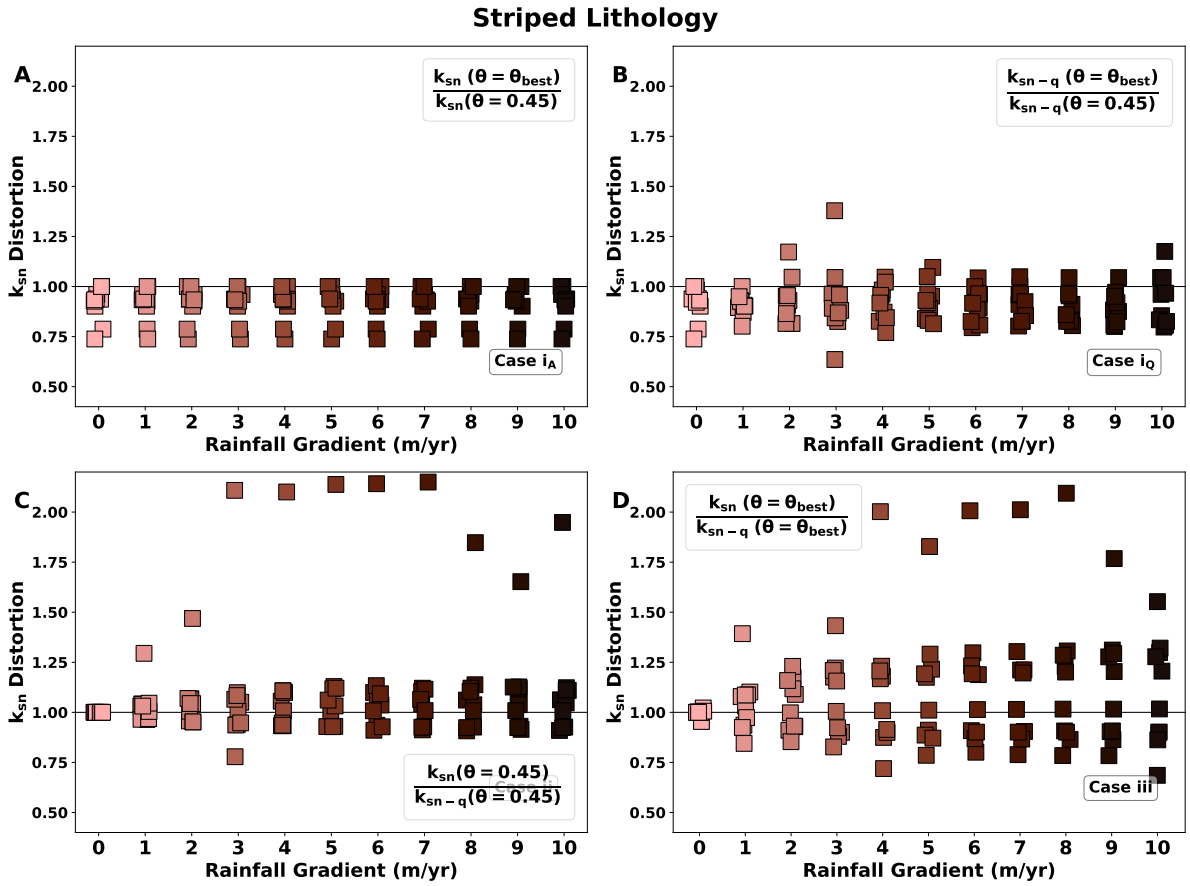

Figure S9. Distortion in k_{sn} for the A-driven incision case under striped lithology and initial m/n=0.45. A distortion of 1 (solid black line) keeps the value of k_{sn} unchanged. We show the possible distortion scenarios that one might encounter under different assumptions of concavity index and incision. (A) shows the distortion incurred by not optimising θ under A-driven incision, whereas (B) highlights the effects of optimising concavity under the incorrect incision scenario (discharge), where we see the largest k_{sn} distortions of up to 115%. (C) keeps concavity index at 0.45 but compares incision scenario and (D) comprises the effects of θ optimisation under different assumptions of incision scenarios.

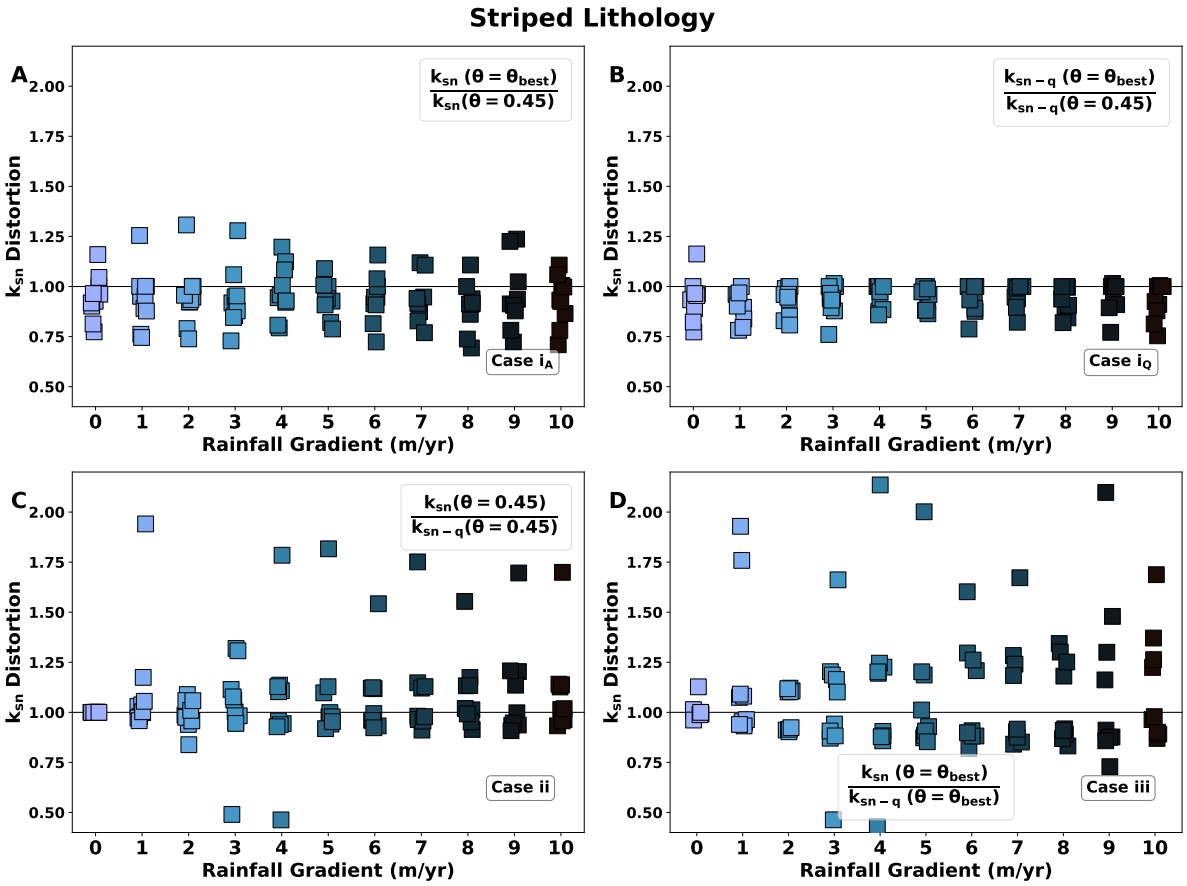

Figure S10. Distortion in k_{sn} for the Q-driven incision case under striped lithology and initial m/n=0.45. A distortion of 1 (solid black line) keeps the value of k_{sn} unchanged. We show the possible distortion scenarios that one might encounter under different assumptions of concavity index and incision. (A) highlights the effects of optimising concavity under the incorrect incision scenario (drainage area), whereas (B) shows the distortion incurred by not optimising θ under Q-driven incision. (C) keeps concavity index at 0.45 but compares incision scenario and (D) comprises the effects of θ optimisation under different assumptions of incision scenarios, where we see the largest k_{sn} distortions of up to 114%.

Table S5. Maximum values of k_{sn} distortion for the striped lithology case with $m/n = 0.45$. Bold values indicate the highest distortion for each incision scenario.

Striped Litho.	Case i_Q	Case i_A	Case ii	Case iii
Drainage Area (A)	38%	26%	**115**%	109%
Discharge (Q)	25%	31%	94%	**114**%

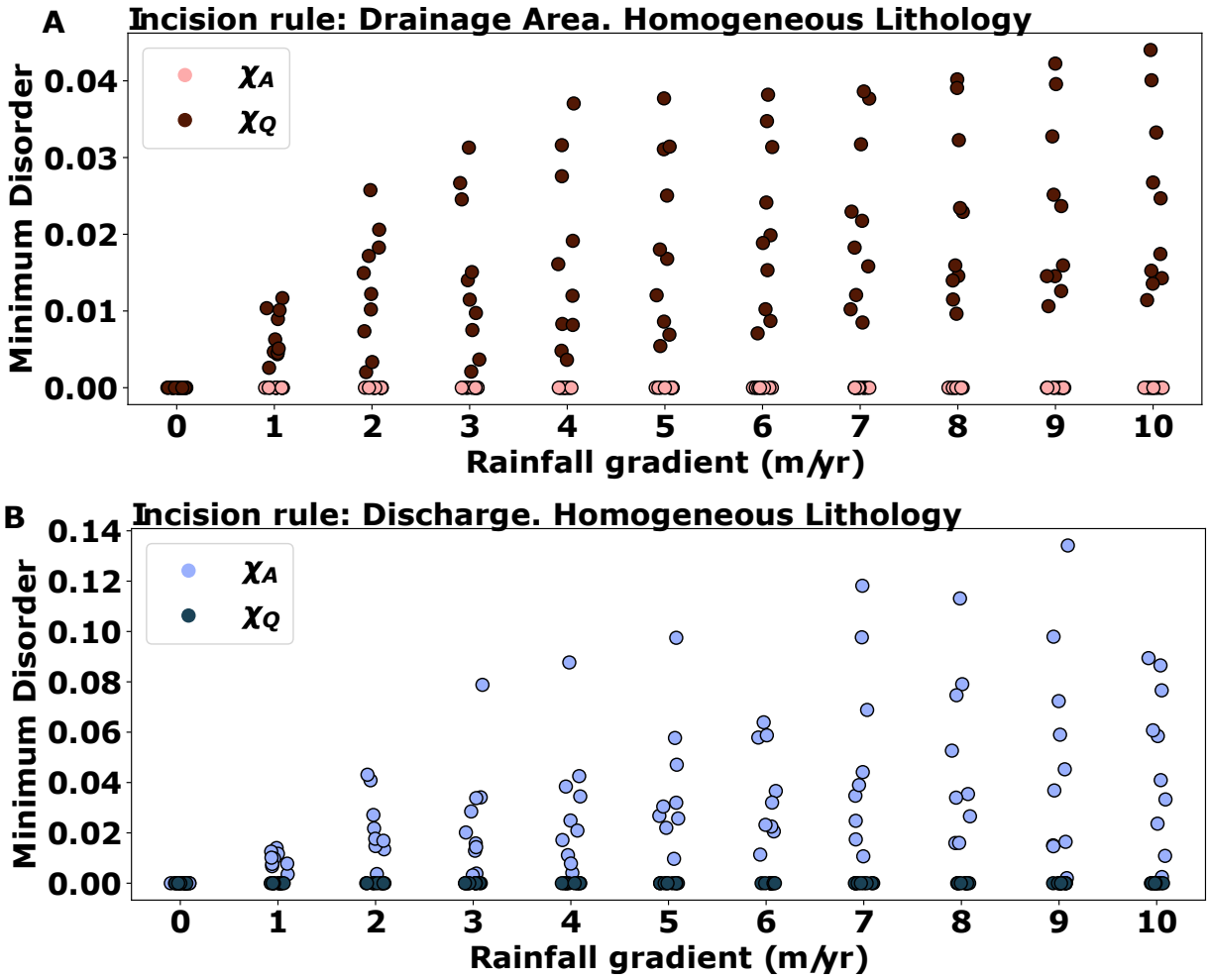

Figure S11. Evolution of the minimum disorder for model runs with a drainage area (A) and a discharge-driven (B) incision rule for a range of rainfall gradients (0-10m/yr) under homogeneous lithology. We show the minimum disorder values when calculating χ_A and χ_Q, for rainfall gradients increases from 0 m/yr to 10 m/yr. The disorder calculated with χ_Q is lower than that calculated with χ_A. The differences become progressively larger as the rainfall gradients increase.

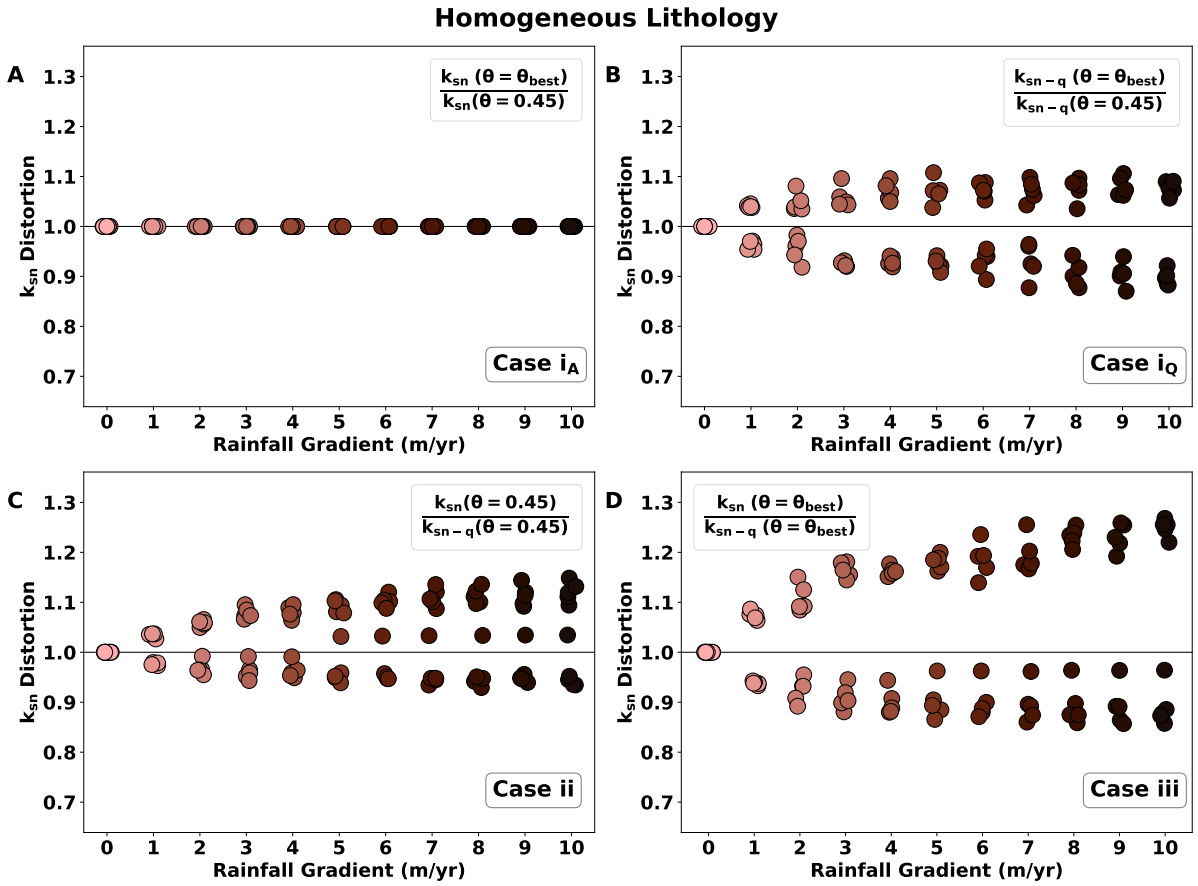

Figure S12. Distortion in k_{sn} for the A-driven incision case under homogeneous lithology and initial m/n=0.45. A distortion of 1 (solid black line) keeps the value of k_{sn} unchanged. (A, Case i_A) indicates that no k_{sn} distortion occurs when the concavity index and the incision case match the model scenario. (B), (C) and (D) show the possible distortion scenarios that one might encounter under different assumptions. (B) highlights the effects of optimising concavity index under an incorrect incision scenario, (C) assumes concavity index is kept at 0.45 but the incision scenario changes and (D) comprises the effects of θ optimisation under different assumptions of incision scenarios, where we see the largest k_{sn} distortions of up to 27%.

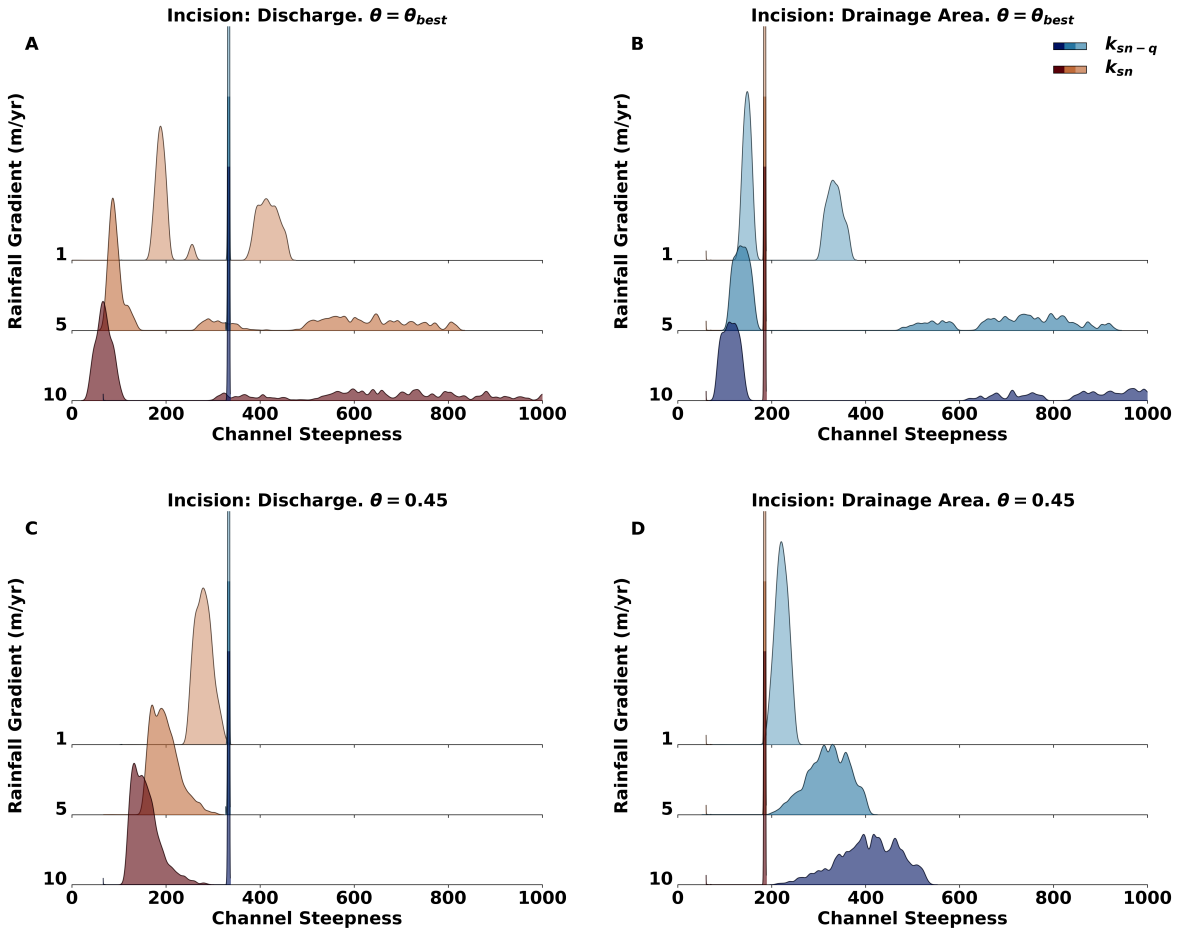

Figure S13. Distribution of k_{sn} and k_{sn-q} values for the basins in the homogeneous lithology simulation. Channel steepness is well constrained when the incision case matches the channel steepness case. The higher the rainfall rate, the larger the distortion in the channel steepness index distributions.

Table S6. Maximum values of k_{sn} distortion for the homogeneous lithology case with $m/n = 0.45$. Bold values indicate the highest distortion for each incision scenario.

Homogeneous Litho.	Case i_Q	Case i_A	Case ii	Case iii
Drainage Area (A)	13%	0%	15%	**27**%
Discharge (Q)	0%	23%	11%	**34**%

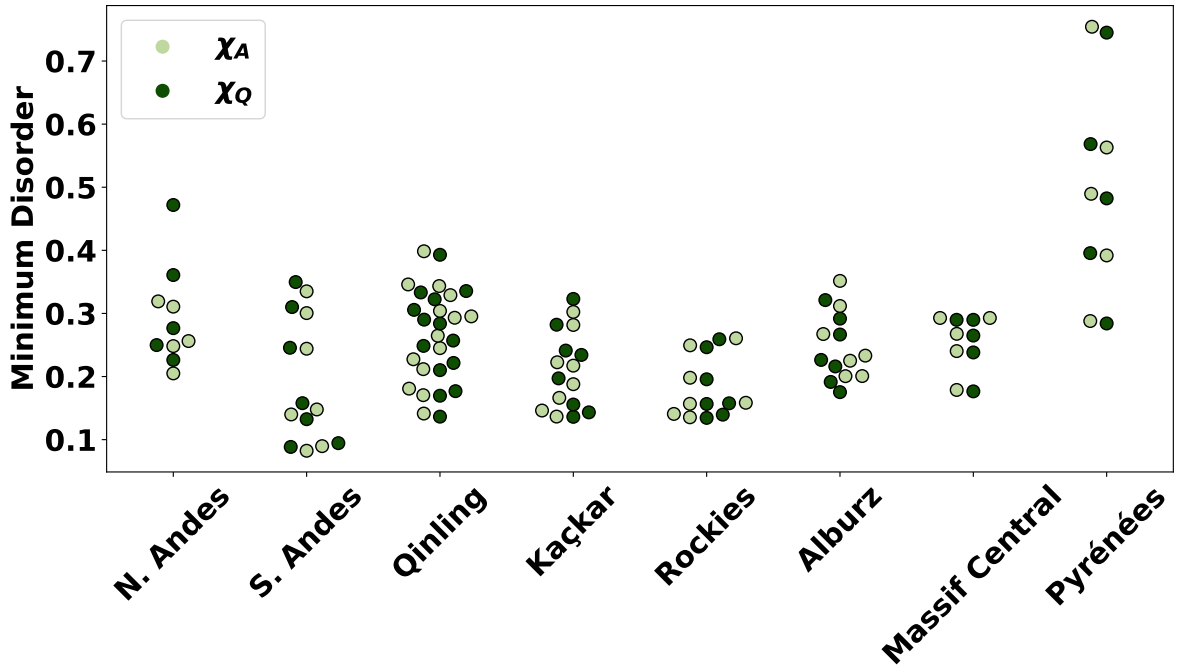

Figure S14. Evolution of the minimum disorder basins in natural landscapes. We show that the minimum D^* values with χ_A and χ_Q have very similar values, making it a challenge to identify the preferential incision route.

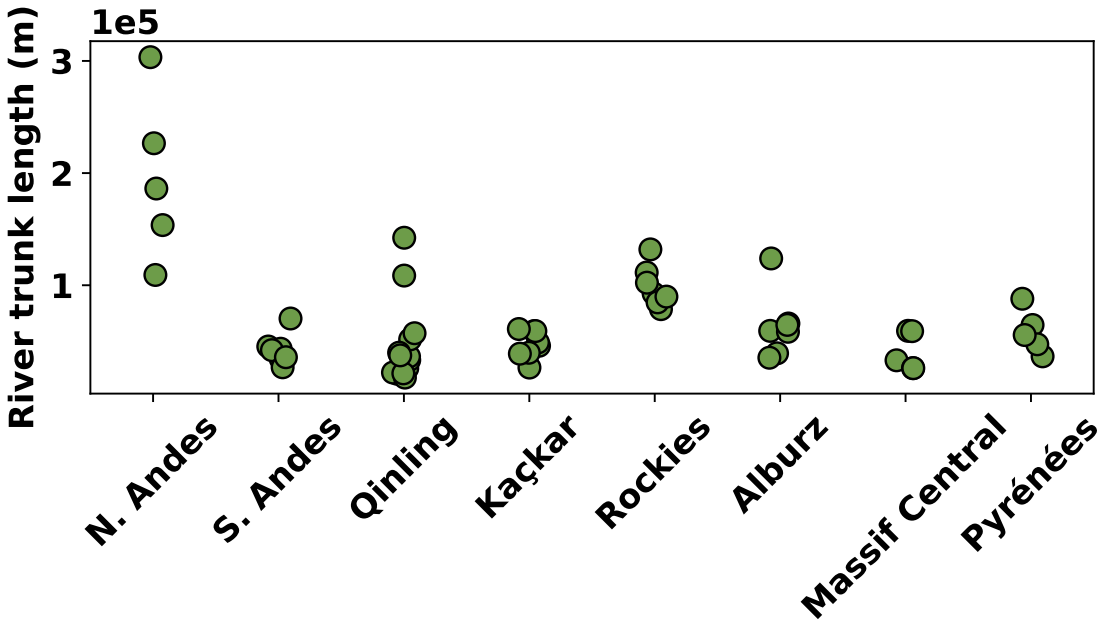

Figure S15. Distribution of the length of the main trunk for the chosen basins in each of the study areas. Areas such as the Northern Andes show a wider range of trunk sizes, from $\sim 100km$ to $> 300km$. Regions such as the Southern Andes or the Kaçkar Mountains all show trunk sizes $< 100km$.

Table S7. Values for the k_{sn} of the basins with maximum distortion in each mountain range under each of the distortion scenarios. Bold values correspond to the case with the highest distortion for each mountain range.

Mountain Range	Case i_A	Case i_Q	Case ii	Case iii
N. Andes	20%	23%	26%	**32**%
S. Andes	56%	26%	**79**%	26%
Qinling	**81**%	50%	28%	33%
Kaçkar	**40**%	38%	15%	14%
Rockies	**47**%	44%	6%	5%
Alburz	**48**%	45%	18%	26%
Massif Central	**48**%	25%	25%	36%
Pyrénées	**67**%	49%	34%	17%

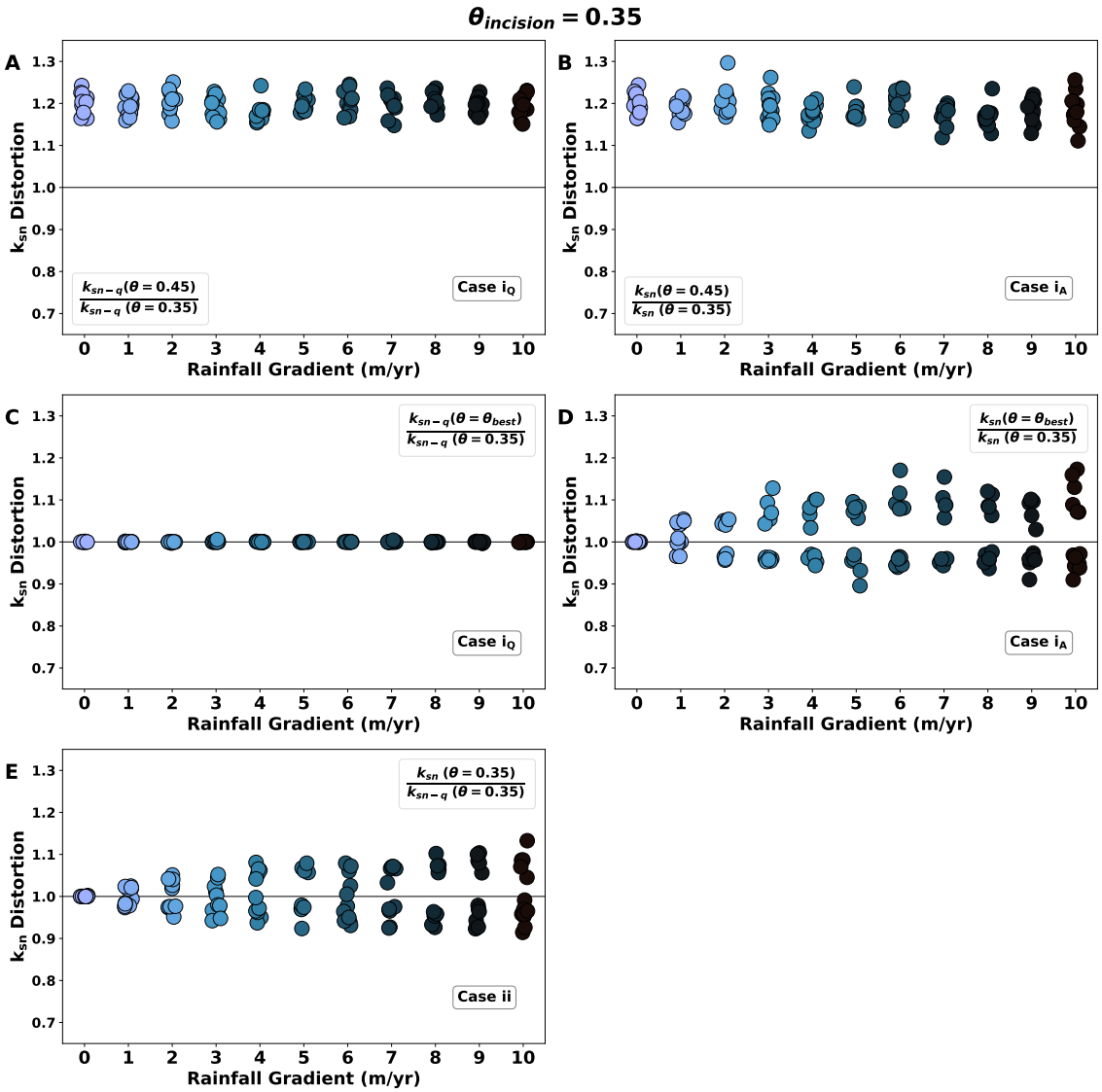

Figure S16. Distortion in k_{sn} for the A-driven incision case under homogeneous lithology and initial m/n=0.35. A distortion of 1 (solid black line) keeps the value of k_{sn} unchanged. (C, Case i_Q) indicates that no k_{sn} distortion occurs when the concavity index and the incision case match the model scenario. (D) highlights the effects of optimising concavity index under an incorrect incision scenario, (A) and (B) assumes that concavity index has been chosen as 0.45 for discharge and drainage area-driven scenarios respectively. (E) assesses the distortion caused by different incision assumptions under the correct concavity index (0.35). We see the largest k_{sn} distortions (up to 30%) in (B).

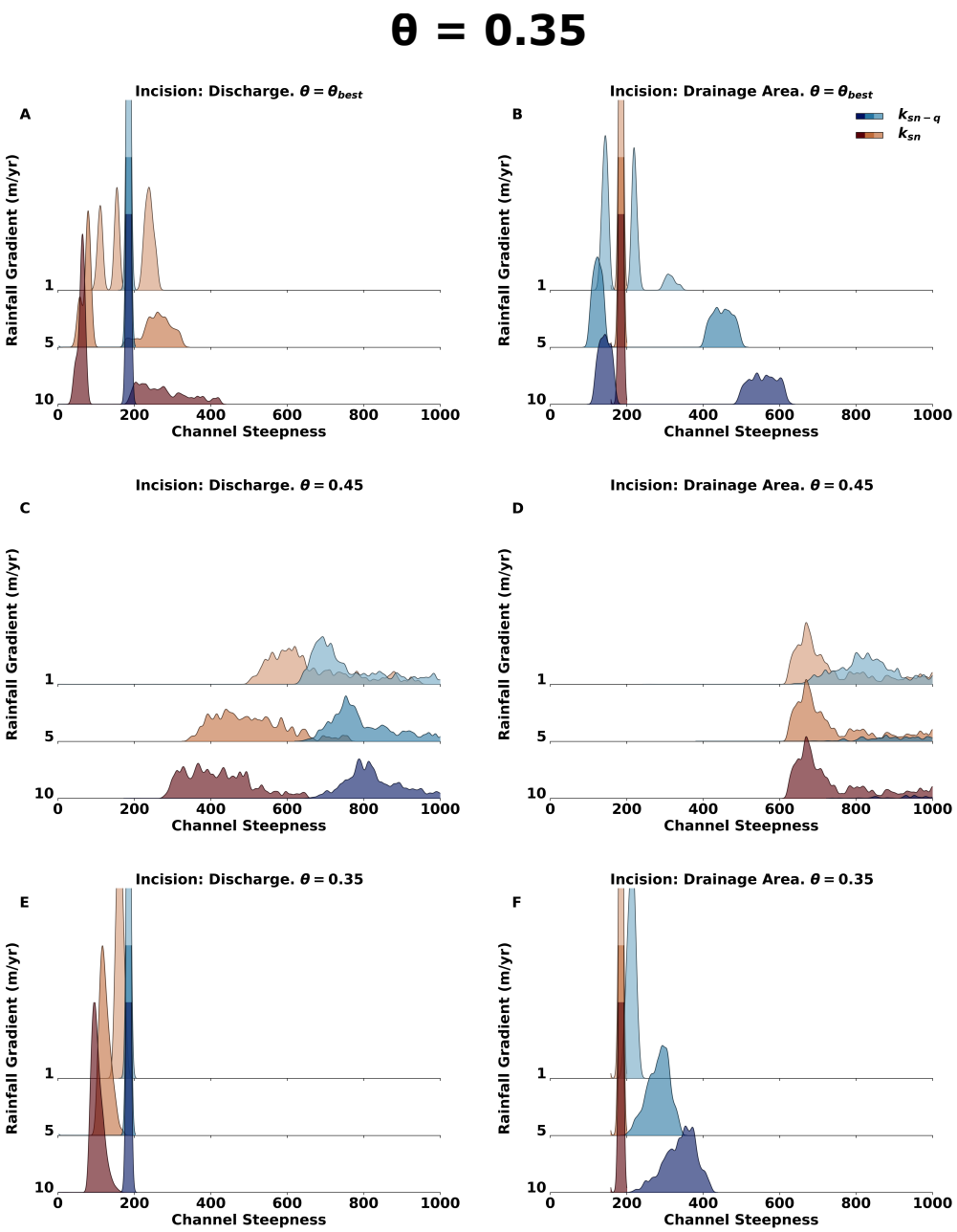

Figure S17. Distribution of k_{sn} and k_{sn-q} values for the basins in the homogeneous lithology simulation with initial concavity of θ=0.35. Channel steepness is well constrained when the incision case matches the channel steepness case. (C) and (D) show the largest deviations from the expected channel steepness distributions. This shows that an incorrect choice of concavity can distort the k_{sn} distributions to a larger extent than rainfall.

Table S8. Maximum values of k_{sn} distortion for the homogeneous lithology case with $m/n = 0.35$. Bold values indicate the highest distortion for each incision scenario.

$m/n = 0.35$	Case $i_{Q,\theta=0.45}$	Case $i_{A,\theta=0.45}$	Case $i_{Q,\theta=\theta_{best}}$	Case $i_{A,\theta=\theta_{best}}$	Case ii
Drainage Area (A)	**26**%	22%	10%	0%	10%
Discharge (Q)	25%	**30**%	1%	17%	13%

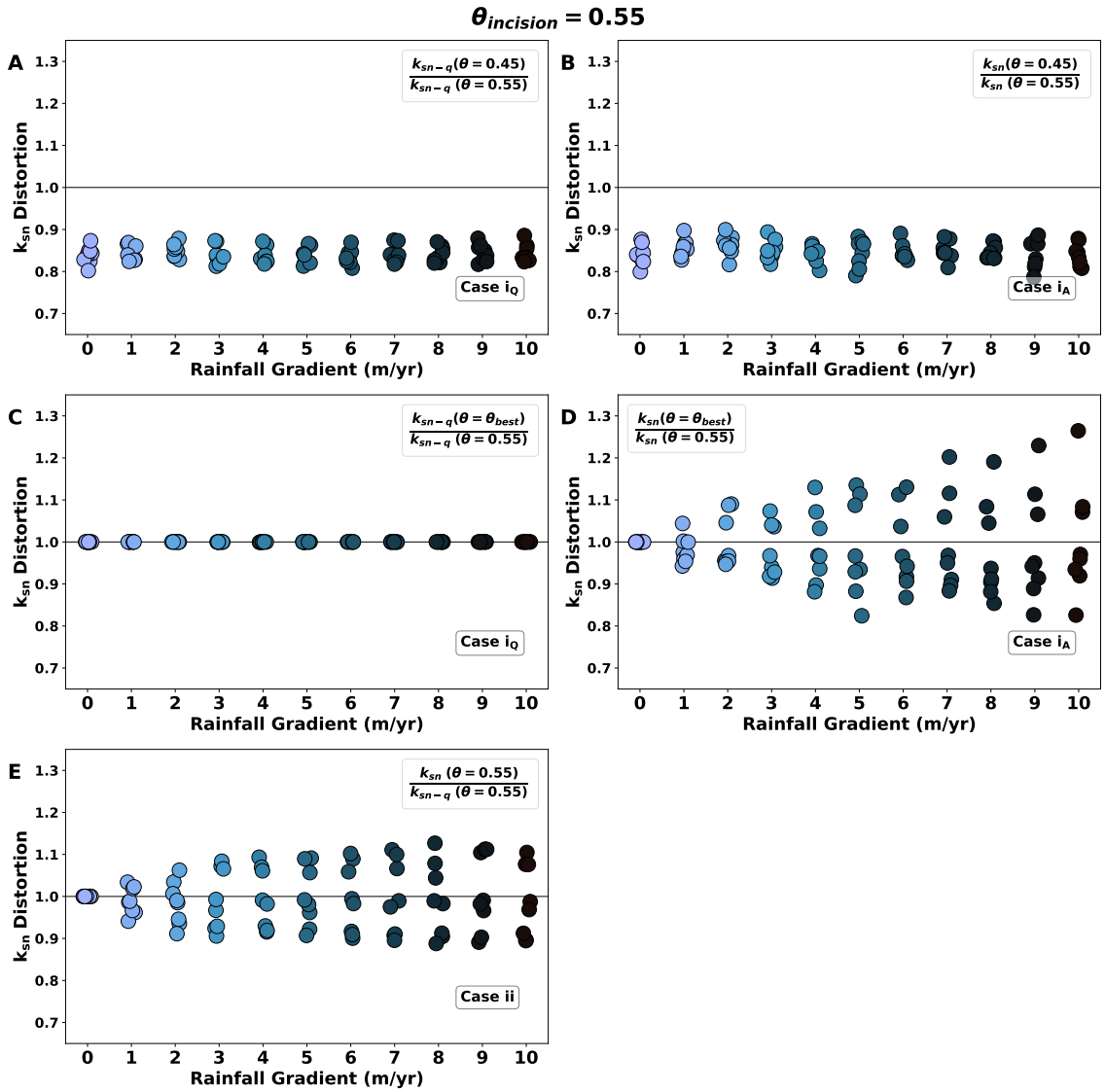

Figure S18. Distortion in k_{sn} for the A-driven incision case under homogeneous lithology and initial m/n=0.55. A distortion of 1 (solid black line) keeps the value of k_{sn} unchanged. (C, Case i_Q) indicates that no k_{sn} distortion occurs when the concavity index and the incision case match the model scenario. (D) highlights the effects of optimising concavity index under an incorrect incision scenario, (A) and (B) assumes that concavity index has been chosen as 0.45 for discharge and drainage area-driven scenarios respectively. (E) assesses the distortion caused by different incision assumptions under the correct concavity index (0.55). We see the largest k_{sn} distortions (up to 26%) in (D).

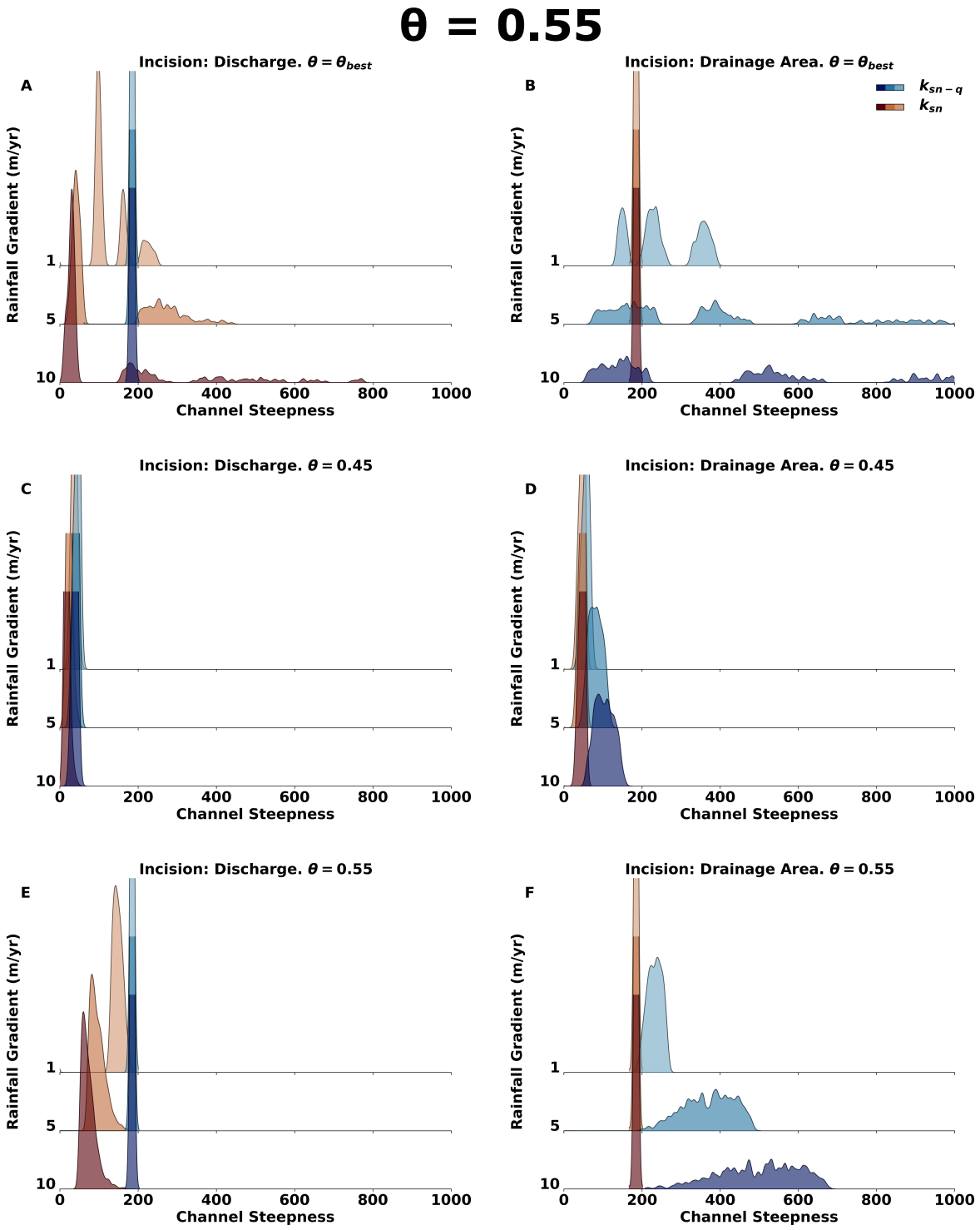

Figure S19. Distribution of k_{sn} and k_{sn-q} values for the basins in the homogeneous lithology simulation with initial concavity of θ=0.55. Channel steepness is well constrained when the incision case matches the channel steepness case.

Table S9. Maximum values of k_{sn} distortion for the homogeneous lithology case with $m/n = 0.55$. Bold values indicate the highest distortion for each incision scenario.

$m/n = 0.55$	Case $i_{Q,\theta=0.45}$	Case $i_{A,\theta=0.45}$	Case $i_{Q,\theta=\theta_{best}}$	Case $i_{A,\theta=\theta_{best}}$	Case ii
Drainage Area (A)	**21**%	17%	18%	0%	10%
Discharge (Q)	20%	21%	0%	**26**%	13%